Inorg. Chem. **2007**, *46*, 1171–1176

New Lanthanide Hybrid as Clustered Infinite Nanotunnel with 3D Ln–O–Ln Framework and (3,4)-Connected Net

You-gui Huang, Ben-lai Wu, Da-qiang Yuan, Yan-qing Xu, Fei-long Jiang, and Mao-chun Hong*

State Key Laboratory of Structure Chemistry, Fujian Institute of Research on the Structure of Matter, Chinese Academy of Sciences, Fuzhou 350002, China

Received August 12, 2006

A series of new lanthanide hybrids $[Ln_3(\mu\text{-}OH)_4(2,5\text{-pydc})(2,5\text{-Hpydc})_3(H_2O)_4]_n$ (Ln = Gd (**1**), Dy (**2**), Er (**3**), Eu (**4**), Sm (**5**), Yb (**6**), Y (**7**); 2,5-pydc=pyridine-2,5-dicarboxylate), as clustered lanthanide oxide ring tunnels with helical dodecahedral chains and fully 3D Ln–O–Ln connectivity, has been hydrothermally synthesized and characterized. The inorganic skeleton of the hybrid can be specified by the Schläfli symbol $(6^210)_2$ (6^410^2) as a single 3D (3,4)-connected net. The luminescence properties have been studied, and the results showed that the Dy(III) (**2**) and Eu(III) (**4**) complexes exhibited sensitized luminescence in the visible region. Variable-temperature magnetic susceptibility measurements of **1**–**6** showed that the complexes **1**–**3** are nearly paramagnets, whereas the depopulation of the Stark levels in complexes **4**–**6** leads to a continuous decrease in μ_{eff} when the sample is cooled from 300 to 2 K.

Introduction

Hybrid inorganic−organic compounds are currently of significant interest and importance, not only because of their fascinating variety of architectures and topologies but also owing to their potential applications, particularly in catalysis, biology, and optical, electronic, and magnetic functional materials.[1] In such materials, functionality can be introduced from either inorganic species or organic linker molecules. Construction of multidimensional M−O−M frameworks has been demonstrated to produce materials cooperative effects and can also lead to improve their thermal stabilities.[2] However, most of the current effort in this area has focused on the design of infinite M−O−M frameworks with d-block transition-metal (TM) ions, thus many hybrids containing multidimensional M−O−M frameworks have been obtained.[3] Unfortunately, in contrast to the above fruitful production of M−O−M frameworks, the design and control over high-dimensional lanthanide-based Ln−O−Ln hybrids are still challenging tasks owing to coordination diversities as well as poor stereochemical preferences of lanthanide ions. Whereas, lanthanides, with their high and variable coordination numbers and flexible coordination geometry, provide unique opportunities for discovery of unusual network topologies,[4] thus leading us to this interesting and challenging field.

We chose pyridine-2,5-dicarboxylate (2,5-pydc) as an organic spacer since this rigid molecule has proven to be able to establish a bridge between metal centers.[5] Herein,

* To whom correspondence should be addressed. E-mail: hmc@ms.fjirsm.ac.cn.

(1) (a) Bowes, C. L.; Qzin, G. A. *Adv. Mater.* **1996**, *8*, 13. (b) Kitagawa, S.; Kondo, M. *Bull. Chem. Soc. Jpn.* **1998**, *71*, 1739. (c) Chui, S. S.-Y.; Lo, M.-F.; Charmant, J. P. H.; Orpen, A. G.; Williams, I. D. *Science* **1999**, *283*, 1148. (d) Kagan, C. R.; Mitzi, D. B.; Dimitrakopoulos, E. D. *Science* **1999**, *286*, 945. (e) Halasyamani, P. S.; Drewitt, M. T.; O'Hare, D. *Chem. Commun.* **1997**, 867. (f) Hagrman, P. J.; Hagrman, D.; Zubieta, J. *Angew. Chem.* **1999**, *111*, 2798; *Angew. Chem., Int. Ed.* **1999**, *38*, 2638.

(2) (a) Livage, C.; Egger, C.; Férey, G. *Chem. Mater.* **1999**, *11*, 1546. (b) Price, D. J.; Tripp, S.; Powell, A. K.; Wood, P. T. *Chem. Eur. J.* **2001**, *7*, 200. (c) Gutschke, S. O. H.; Price, D. J.; Powell, A. K.; Wood, P. T. *Angew. Chem.* **2001**, *113*, 1974; *Angew. Chem., Int. Ed.* **2001**, *40*, 1920. (d) Guillou, N.; Gao, P. M.; Forster, P. M.; Chang, J. S.; Park, S. E.; Férey, G.; Cheetham, A. K. *Angew. Chem.* **2001**, *113*, 2913; *Angew. Chem., Int. Ed.* **2001**, *40*, 2831.

(3) (a) Guillou, N.; Livage, C.; Drillon, M.; Férey, G. *Angew. Chem., Int. Ed.* **2003**, *42*, 5314. (b) Forster, P. M.; Cheetham, A. K. *Angew. Chem., Int. Ed.* **2002**, *41*, 457. (c) Schmitt, W.; Hill, J. P.; Juanico, M. P.; Caneschi, A.; Costantino, F.; Anson, C. E.; Powell, A. K. *Angew. Chem., Int. Ed.* **2005**, *44*, 4187. (d) Xiang, S. C.; Wu, X. T.; Zhang, J. J.; Fu, R. B.; Hu, S. M.; Zhang, X. D. *J. Am. Chem. Soc.* **2005**, *127*, 16352. (e) Sudik, A. C.; Côté, A. P.; Yaghi, O. M. *Inorg. Chem.* **2005**, *44*, 2998. (f) Rosi, N. L.; Kim, J.; Eddaoudi, M.; Chen, B.; O'Keeffe, M.; Yaghi, O. M. *J. Am. Chem. Soc.* **2005**, *127*, 1504.

(4) (a) Long, D. L.; Blake, A. J.; Champness, N. R.; Wilson, C.; Schröder, M. *Angew. Chem., Int. Ed.* **2001**, *40*, 2443. (b) Long, D. L.; Blake, A. L.; Champness, N. R.; Hubberstey, P.; Proserpio, D. M.; Wilson, M. *Angew. Chem., Int. Ed.* **2004**, *43*, 1851. (c) Cui, Y.; Ngo, H. L.; White, P. S.; Lin, W. *Chem. Commun.* **2002**, 1666. (d) Qin, C.; Wang, X. L.; Wang, E. B.; Su, Z. M. *Inorg. Chem.* **2005**, *44*, 7122. (e) Zhang, M. B.; Zhang, J.; Zheng, S. T.; Yang, G. Y. *Angew. Chem., Int. Ed.* **2005**, *44*, 1385.

10.1021/ic0615271 CCC: $37.00
Published on Web 01/13/2007

we report the systematic syntheses, structures, visible luminescence, and magnetic properties of a series of new lanthanide hybrids, generally formulated as $[Ln_3(\mu\text{-}OH)_4(2,5\text{-}pydc)(2,5\text{-}Hpydc)_3(H_2O)_4]_n$ (Ln = Gd (**1**), Dy (**2**), Er (**3**), Eu (**4**), Sm (**5**), Yb (**6**), Y (**7**)). These structures contain trigonal dodecahedral helical chains and clustered lanthanide oxide ring tunnels which have never been reported up until now. To the best of our knowledge, **1**−**7** are the first lanthanide carboxylates with fully 3D Ln−O−Ln connectivity as well as the vertex symbol $(6^210)_2(6^410^2)$ which has never been documented for metal-organic frameworks (MOFs).

Experimental Section

All chemicals are analytical grade and used without further purification. The hydrothermal reaction was performed in a 25 mL Teflon-lined stainless steel autoclave under autogenous pressure. Infrared spectra were recorded on a Magna 750 FR−IR spectrometer using KBr pellets. C, H, and N microanalyses were measured with an elemental Vairo EL analyzer. Powered X-ray diffraction (XRD) patterns of the samples were recorded by an X-ray diffractometer (RIGAKU-DMAX2500) with Cu Kα radiation. Thermal analyses were performed using a thermal analyst 2100TA Instrument and a SDT 2960 Simultaneous TGA-DTA Instrument. Fluorescence spectra were measured at room temperature on an Edinburgh FL-FS920 TCSPC system. In the measurements of emission and excitation spectra, the slit width was 1.5 mm and the scan rate is 1 nm/s. An Edinburgh Xe900 xenon arc lamp was used as an exciting light source with delay time 1−2 μs. The polycrystalline magnetic susceptibility data were collected on a Quantum Design PPMS model 6000 magnetometer in the temperature range from 2 to 300 K.

Synthesis of the Complexes. All seven complexes were prepared by the same method, as follows: A mixture of Ln_2O_3 (0.1 mmol) and H_2pydc (0.024 g, 0.15 mmol) in H_2O (10 mL) was adjusted to pH = 4 with HCl, sealed in a 25 mL Teflon-lined bomb at 160 °C for 3 days, and then slowly cooled to room temperature at a cooling rate of 5 °C/h. Colorless prismatic crystals (pink for complex **3**) were recovered by filtration, washed by distilled water, and air-dried (Yield: 63%, 55%, 72%, 68%, 60%, 76%, and 80% based on H_2pydc for **1**−**7**, respectively). The positions of the diffraction peaks of the experimental and simulated XRD patterns correspond well, thus indicating phase purity of the as-synthesized samples (Figure S5). Elemental analysis calcd (%) for $C_{28}H_{27}Gd_3N_4O_{24}$ (**1**): C 26.37, H 2.12, N 4.40; found: C 26.34, H 2.11, N 4.42; $C_{28}H_{27}Dy_3N_4O_{24}$ (**2**): C 25.85, H 2.08, N 4.31; found: C 25.81, H 2.05, N 4.30; $C_{28}H_{27}Er_3N_4O_{24}$ (**3**) C 25.77, H 2.07, N 4.29; found C 25.78, H 2.05, N 4.25. $C_{28}H_{27}Eu_3N_4O_{24}$ (**4**): C 26.69, H 2.14, N 4.45; found: C 26.65, H 2.11, N 4.42; $C_{28}H_{27}Sm_3N_4O_{24}$ (**5**): C 26.81, H 2.15, N 4.47; found: C 26.80, H 2.13, N 4.44; $C_{28}H_{27}Yb_3N_4O_{24}$ (**6**): C 25.42, H 2.04, N 4.24; found: C 25.41, H 2.06, N 4.26; $C_{28}H_{27}Y_3N_4O_{24}$ (**7**): C 31.40, H 2.52, N 5.23; found: C 31.38, H 2.53, N 5.25. IR for **1** (KBr cm^{-1}) 3408(s), 1738(m), 1638(s), 1455(m), 1337(m), 812(w), 750(m), 691(m), 617(m), 524(w); for **2** 3439(s), 1727(m), 1625(s), 1614(s), 1540(m), 1349(m), 814(w), 758(m), 696(m), 617(m), 516(w); for **3** 3410(s), 1736(m), 1640(s), 1452(m), 1341(m), 815(w), 753(m), 691(m), 615(m), 524(w); for **4** 3400(s), 1748(m), 1633(s), 1453(m), 1336(m), 812(w), 752(m), 693(m), 617(m), 526(w); for **5** 3403(s), 1743(m), 1635(s), 1458(m), 1339(m), 816(w), 753(m), 690(m), 614(m), 521(w); for **6** 3406(s), 1745(m), 1638(s), 1452(m), 1335(m), 812(w), 756(m), 693(m), 619(m), 526(w); for **7** 3404(s), 1736(m), 1641(s), 1618(s), 1540(m), 1372(m), 818(w), 758(m), 692(m), 621(m), 509(w). Thermogravimetric analyses (TGA) indicate that **1**−**7** are stable in N_2 up to 150 °C. Between 150 and 330 °C, weight loss corresponding to loss of coordinated H_2O and μ-OH groups is observed, and loss corresponding to 2,5-H_2pydc ligands occurs between 420 and 700 °C (Figure S6).

X-ray Crystallography. Data collections were performed at 293(2) K on a Siemens SMART CCD (**5**) or Mercury CCD (**1**−**4** and **7**) diffractometer with graphite monochromated Mo−Kα radiation (λ = 0.71073 Å). (For complex **6**, a suitable crystal was selected for X-ray diffraction analysis, whereas the data were not collected. The cell parameters of **6** are as follows: $a = b = 14.846(3)$, $c = 14.604(4)$ Å, $\alpha = \beta = \gamma = 90°$; and its experimental XRD pattern corresponds well with the simulated XRD pattern of **4**, so it is sure that complex **6** is isostructural with **4**.) The structures were solved by direct methods, and all calculations were performed using the SHELXL package.[7] The structures were refined by full matrix least-squares with anisotropic displacement parameters for non-hydrogen atoms. In addition, the pyridine N atom in **1**−**5** and **7** is disordered, and the atom is split into two partial atomic positions with a refined occupancy of 0.5. All hydrogen atoms belonging to the water molecules and μ-OH groups were found in the electron density map and refined isotropically. The other H atoms were generated geometrically and treated as riding. The crystallographic data are summarized in Table 1, selected bond lengths and angles of complex **4** are listed in Tables 2, and the bond lengths and angles of the other complexes are listed in Tables S1−S5 in the Supporting Information. CCDC-613180 (**1**), 613181 (**2**), 602307 (**3**), 602305 (**4**), 602306 (**5**), and 613182 (**7**) contain the crystallographic data for this paper (Supporting Information).

Results and Discussion

Prismatic crystals of **1**−**7** were obtained by hydrothermal reactions of Ln_2O_3 and H_2pydc in water adjusted with HCl (pH = 4). X-ray crystal structure analyses reveal that **1**−**7** are isostructural and crystallize in the high-symmetry space group $I4_1/a$. Therefore, the structure of **4** is selected and described in detail to represent their frameworks.

Crystal Structure of Complex 4. An X-ray diffraction study performed on complex **4** reveals that each asymmetric unit contains two crystallographically unique Eu^{III} ions. Both Eu1 and Eu2 are eight-coordinated in the shape of distorted trigonal dodecahedron. Eu1 is coordinated by four cis carboxylate oxygen atoms from four 2,5-pydc ligands and by four trans μ-OH groups; while Eu2 is coordinated by one μ-OH group, one aqua oxygen atom, and four carboxylate oxygen atoms, and the remnant two sites of Eu2 are occupied by two pyridyl nitrogens from 2,5-pydc ligands (Figures 1 and S1). The Eu−O bond distances range from 2.362 to 2.586 Å, while the Eu−N bond lengths are slightly longer ranging from 2.549 to 2.617 Å. The coordination modes of pentacoordinating 2,5-Hpydc in **4** are shown in Scheme 1. The carboxylate groups in 2,5-Hpydc ligand are partially

(5) (a) García-Zarracino, R.; Höpfl, H. *Angew. Chem., Int. Ed.* **2004**, *43*, 1507. (b) Humphrey, S. M.; Wood, P. T. *J. Am. Chem. Soc.* **2004**, *126*, 13236. (c) Liu, Y. L.; Kravtsov, V. C.; Bearchamp, D. A.; Eubank, J. F.; Eddaoudi, M. *J. Am. Chem. Soc.* **2005**, *127*, 7266.;

(6) Chen, J. W.; Zhang, J.; Zheng, S. T.; Zhang, M. B.; Yang, G. Y. *Angew. Chem., Int. Ed.* **2006**, *45*, 73.

(7) Sheldrick, G. M. *SHELXTL-97, Program for the Solution of Crystal Structures*; University of Göttingen: Germany 1997.

Table 1. Crystal Data for **1**−**5** and **7**

compound	**1**	**2**	**3**	**4**	**5**	**7**
formula	$C_{28}H_{27}Gd_3N_4O_{24}$	$C_{28}H_{27}Dy_3N_4O_{24}$	$C_{28}H_{27}Er_3N_4O_{24}$	$C_{28}H_{27}Eu_3N_4O_{24}$	$C_{28}H_{27}Sm_3N_4O_{24}$	$C_{28}H_{27}N_4O_{24}Y_3$
Fw	1275.29	1291.04	1361.36	1259.36	1262.53	1070.27
crystal size [mm]	0.20 × 0.15 × 0.08	0.20 × 0.18 × 0.08	0.30 × 0.20 × 0.20	0.35 × 0.10 × 0.05	0.30 × 0.25 × 0.15	0.40 × 0.35 × 0.12
crystal system	tetragonal	tetragonal	tetragonal	tetragonal	tetragonal	tetragonal
space group	$I4_1/a$	$I4_1/a$	$I4_1/a$	$I4_1/a$	$I4_1$/a	$I4_1/a$
a [Å]	15.0339(7)	14.9695(8)	14.8150(8)	14.9759(7)	15.0751(6)	14.9579(8)
c [Å]	14.7107(13)	14.6577(16)	14.6396(14)	14.7310(13)	14.7426(7)	14.6505(15)
V [Å^3]	3324.9(4)	3284.6(4)	3213.2(4)	3303.8(4	3350.4(2)	3277.9(4)
Z	4	4	4	4	4	4
ρ_{calcd} [g cm^{-3}]	2.548	2.611	2.814	2.518	2.489	2.169
μ [mm^{-1}]	6.027	6.868	7.890	5.738	5.304	5.381
T [K]	293	293	293	293	293	293
λ(Mo$_{K\alpha}$) [Å]	0.71073	0.71073	0.71073	0.71073	0.71073	0.71073
reflcns collected	12363	12316	9286	12343	9001	12521
unique reflcns	1900	1883	1745	1892	1588	1881
observed reflcns	1866	1857	1677	1823	1504	1757
parameters	138	138	138	139	138	138
S on F^2	1.275	1.245	1.149	1.264	1.224	1.163
R_1[a]	0.0599	0.1038	0.0645	0.0478	0.0520	0.0751
R_w[b]	0.1287	0.2395	0.1277	0.1058	0.1482	0.1953
$\Delta\rho$ min and max [e Å^{-3}]	1.557 and −2.299	2.842 and −4.162	1.326 and −2.318	1.355 and −1.067	0.887 and −1.264	0.739 and −2.068

[a] $R = \Sigma||F_0| - |F_c||/\Sigma|F_0|$. [b] $R_w = [\Sigma w(F_0^2 - F_c^2)^2/\Sigma w(F_0^2)^2]^{1/2}$.

Table 2. Selected Bond Lengths [Å] and Angles [deg] for **4**[a]

bond			
Eu1−EnDashEnDashO1	2.377 (4)	Eu2−O6	2.523 (6)
Eu1−O5	2.446 (5)	Eu2−N1D	2.541 (6)
Eu2−O5	2.358 (5)	Eu2−O3F	2.587 (7)
Eu2−O2A	2.443 (5)	Eu2−O2D	2.589 (6)
Eu2−O3E	2.446 (5)	Eu2−N2F	2.611 (6)
angle			
O1B−Eu1−O1A	129.62 (1)	O2A−Eu2N1D	74.45 (2)
O1B−Eu1−O1	74.0 (2)	O3E−Eu2−N1D	138.3 (2)
O1B−Eu1−O5B	72.83 (2)	O6−Eu2−N1D	138.46 (2)
O1A−Eu1−O5B	146.52 (2)	O5−Eu2−O3F	157.30 (2)
O1−Eu1−O5B	76.11 (2)	O2A−Eu2−O3F	76.23 (2)
O1C−Eu1−O5B	72.62 (2)	O3E−Eu2−O3F	122.19 (2)
O5B−Eu1−O5	140.8 (2)	O6−Eu2O3F	79.67 (2)
O5B−Eu1−O5A	96.45 (8)	N1D−Eu2−O3F	72.52 (2)
O5−Eu2−O2A	81.76 (2)	O5−Eu2−O2D	80.2 (2)
O5−Eu2−O3E	73.96 (2)	O2A−Eu2−O2D	126.14 (1)
O2A−Eu2−O3E	143.65 (2)	O3E−Eu2−O2D	76.1 (2)
O5−Eu2−O6	87.50 (2)	O6−Eu2−O2D	157.84 (2)
O2A−Eu2−O6	69.30 (2)	N1D−Eu2−O2D	63.40 (2)
O3E−Eu2−O6	82.8 (2)	O3F−Eu2−O2D	117.51 (2)
O5−Eu2−C7D	106.92 (2)	O5−Eu2−N2F	140.11 (2)
O2A−Eu2−C7D	74.45 (2)	O2A−Eu2−N2F	137.42 (2)
O5−Eu2−N1D	106.92 (2)	O3E−Eu2−N2F	73.59 (2)
O2A−Eu2−N1D	74.45 (2)	O6−Eu2−N2F	110.66 (2)
O3E−Eu2−N1D	138.3 (2)	N1D−Eu2−N2F	83.15 (2)
O6−Eu2−N1D	138.46 (2)	O3F−Eu2−N2F	62.54 (2)
O5−Eu2−N1D	106.92 (2)	O2D−Eu2−N2F	70.03 (2)

[a] Symmetry codes: A: 5/4 − x, −1/4 + y, 1/4 − z; B: 1 − x, 3/2 − y, z; C: 1/4 + x, 5/4 − y, 1/4 − z; D: x − 1/2, y, 1/2 − z; E: 1 − x, 1 − y, 1 − z; F: −1/4 + x, 3/4 − y, 3/4 − z.

deprotonated, which can be verified by the presence of characteristic bands at about 1730 cm^{-1} in IR spectrum.[8] The analogous phenomenon was also observed in [Ln(pydc)(Hpydc)]$_n$ which is a 3-D coordination polymer with rutile topology.[4d] It should be mentioned at this point that even though the synthetic procedure of [Ln$_3$(μ-OH)$_4$(2,5-pydc)(2,5-Hpydc)$_3$(H$_2$O)$_4$]$_n$ and [Ln(pydc)(Hpydc)]$_n$ are identical with the exception of HCl used to adjust the pH value; their

(8) Bellamy, L. J. *The Infrared Spectra of Complex Molecules*; Wiley: New York, 1958.

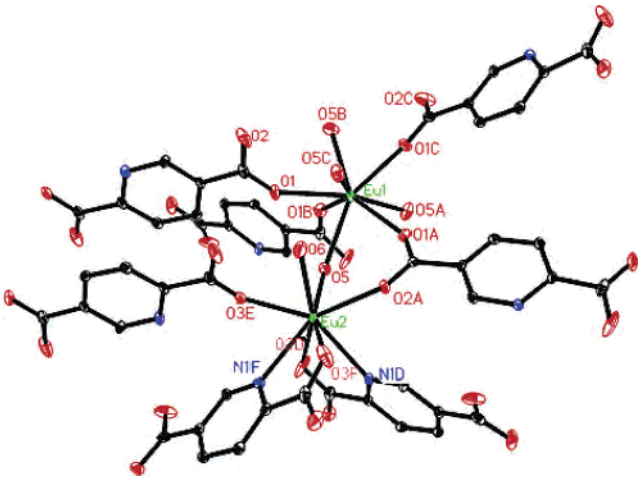

Figure 1. The coordination environments of Eu1 and Eu2 atoms in **4**. Symmetry codes: A: 5/4-x, −1/4+y, 1/4-z; B: 1−x, 3/2-y, z; C: 1/4+x, 5/4-y, 1/4-z; D: x-1/2, y, 1/2-z; E: 1-x, 1-y, 1-z; F: −1/4+x, 3/4-y, 3/4-z, respectively.

Scheme 1. Coordination Modes of 2,5-Hpydc Lignads in the Structure of **4**

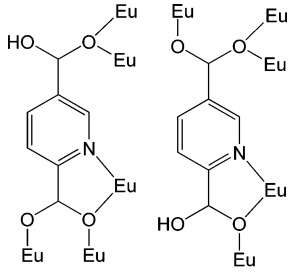

topologies are fully different, illustrating the important role of pH value on the identity of the products in synthesis. The assignment of the oxidation states for the Eu atoms is consistent with the charge and confirmed by bond valence sum calculations. The valence sums[9] ($\Sigma s = \exp\Sigma[(Ro-R)/0.37]$, Ro = 2.074 for Eu−O and 2.240 for Eu−N respec-

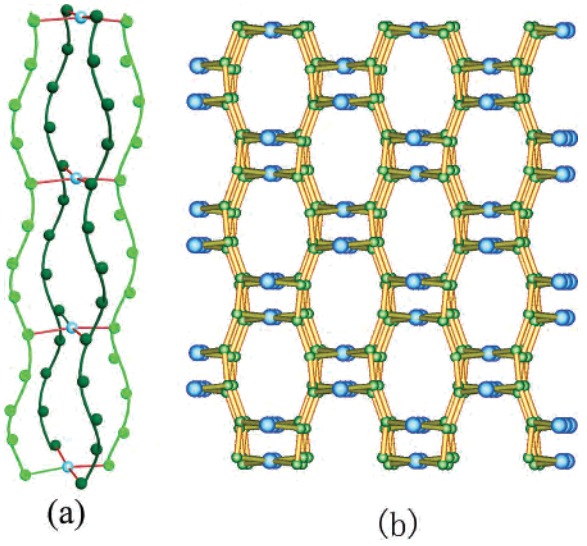

Figure 2. (a) View of four helixes with opposite chiralities, green (right-handed helixes) olive (left-handed helixes). (b) View of the $(6^210)_2(6^410_2)$ topology of the 3D inorganic skeleton. The two types of nodes and links in **4** are differentiated by color (blue and green spheres represent Eu1 and Eu2 atoms, respectively; olive and yellow bonds represent Eu1−Eu2 and Eu2−Eu2 linkers, respectively).

tively, R = Eu−O or Eu−N distance in Å) for the two Eu atoms are 2.79 and 3.22, respectively, which are in good agreement with the expected bond valence of 3.00.

Eu1 locates on the fourfold inversion axes and Eu2 on the fourfold screw axes. Each Eu2 is doubly bridged by μ-O_2 and μ-O_3 to two adjacent Eu2 with the Eu−O−Eu angles in the range of 102.63−102.77° and further bridges to one Eu1 via μ-OH and O1−C−O2 carboxylate moiety in syn−syn fashion. This, therefore, defines a three-connecting node within the structure. Each Eu1 connects to four adjacent Eu2, consequently defining a four-connecting node. Each Eu2 dodecahedron shares edges with two adjacent Eu2 to give dodecahedral helices running along the *c*-axis. The helices with opposite chirality are arranged alternately along *a* and *b* axes (Figure 2a). Each fourfold inversion axis running through Eu1 connects with four adjacent helices, and each helix also connects with four adjacent fourfold inversion axes, which generates an unprecedented 3-D framework with achiral channels and corrugated 12-membered wheels (Figure 3). The Ln wheels reported earlier either live alone as isolated clusters[10] or extend by sharing bridges forming layered cluster network.[6] Notably, the arraying mode of the wheel-shaped $\{Eu_{12}\}$ clusters here in **4** is significantly different from the above ones. The Ln wheels intersect each other to generate a 3D inorganic skeleton with fully 3D Ln−O−Ln connectivity and ring lanthanide oxide tunnels along *a* and *b* axial directions (Figures 4, S3, and S4). The tunnels above connect with each other forming an intersecting 3D pore.

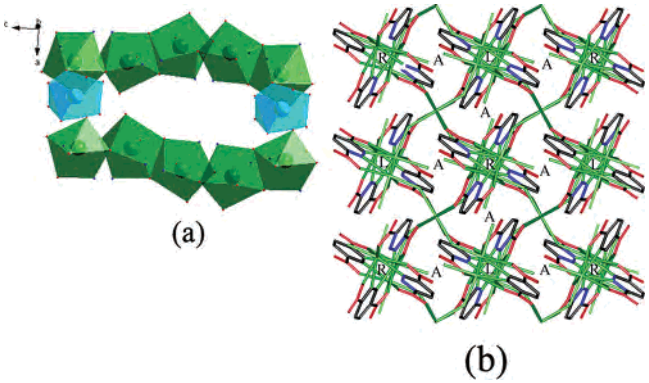

Figure 3. (a) Polyhedron view of a corrugated 12-membered lanthanide wheel (blue and green polyhedrons represent Eu1 and Eu2 atoms, respectively). (b) View of the 3D network down the *c*-axis for **4**.

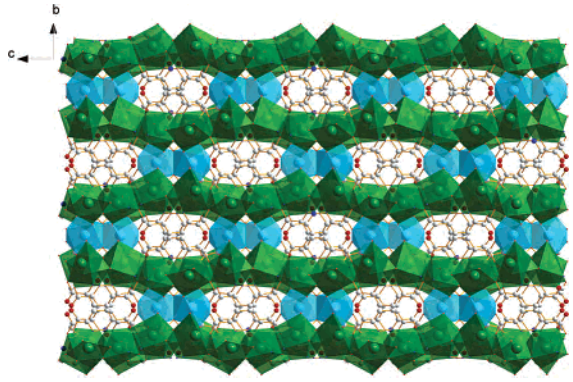

Figure 4. View of the ring lanthanide oxide nanotunnel down the *a*-axis for **4** (blue and green polyhedrons represent Eu1 and Eu2 atoms, respectively).

Remarkably, 2,5-pydc ligands are trapped in the inner of the tunnels producing polar regions surrounding the lanthanide oxide walls and nonpolar regions surrounding tunnels. Although the 2,5-pydc ligand has more than 13 coordination modes,[4d] it adopts a unique μ_5-pydc mode only in **4**, and the unique μ_5-pydc mode plays a key role in formation and stabilizing the lanthanide oxide tunnels.

Better insight into the nature of this intricate lanthanide oxide framework can be achieved by the application of a topological approach, i.e., reducing multidimensional structures to simple node-and-connecting nets. As discussed above, the framework is composed of planar four-connecting (Eu1) and triangular three-connecting (Eu2) nodes. Wells[11] classified such networks as nonuniform (3,4)-connected net where 3 and 4 indicate the connectivity of the nodes. As a nonuniform net, there is more than one kind of shortest circuits of these nodes. Wells found and described two types of nonuniform (3,4)-connected nets: Ge_4N_3 and $N(CH_3)_4F\cdot 4H_2O$.[11] Between the two structure types, the Ge_4N_3 topology has often been observed in complex oxides and fluorides, such as Be_2GeO_4, Li_2BeF_4, etc. To the best of our knowledge, however, the network topology of **4** is unprecedented in either complex oxides or MOFs. The net of **4** can further be described as a metal-organic analogous to the above-mentioned $N(CH_3)_4F\cdot 4H_2O$, in which the water molecules are located in a 4-fold screw axis as 3-connected node, and

(9) Brese, N. E.; O'Keeffe, M. *Acta Crystallogr., Sect. B*: *Struct. Sci.* **1991**, *47*, 192. (b) Brown, D. I.; Altermatt, D. *Acta Crystallogr., Sect. B*: *Struct. Sci.* **1985**, 41 244.

(10) (a) Wang, R. Y.; Zheng, Z. P.; Jin, T. Z.; Staples, R. J. *Angew. Chem., Int. Ed.* **1999**, *38*, 1813. (b) Wang, R. Y.; Selby, H. D.; Hui, L.; Carducci, M. D.; Jin, T. Z.; Zheng, Z. P.; Anthis, J. W.; Staples, R. J. *Inorg. Chem.* **2002**, *41*, 278. (c) Xu, J. D.; Raymond, K. N. *Angew. Chem., Int. Ed.* **2000**, *39*, 2745. (d) Westin, L. G.; Kritikos, M.; Caneschi, A. *Chem. Commun*. **2003**, 1012.

(11) Mclean, W. J.; Jeffrey, G. A. *J. Chem. Phys.* **1957**, *47*, 414.

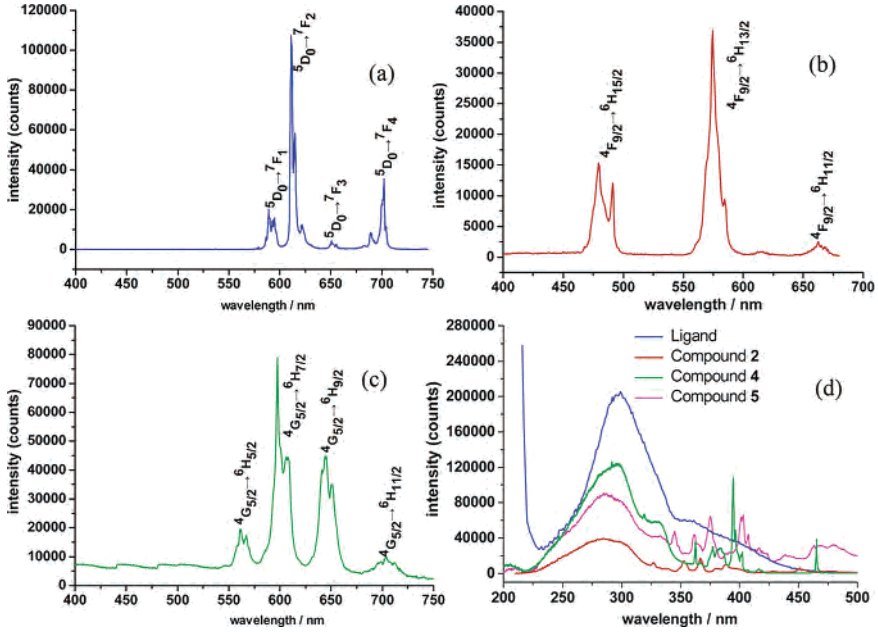

Figure 5. Solid-state excitation (d) and emission spectra for **4**(a), **2**(b), and **5**(c) at room temperature (excitation at 296, 285, and 302 nm for **4**, **2**, and **5**, respectively).

the N^+ and F^- lie alternately along a 4-fold inversion axis as 4-connected nodes. In $N(CH_3)_4F{\cdot}4H_2O$, the coordination of the 4-connected node is intermediate between the planar and tetrahedral, while in **4** that is exactly planar. Among the known (3,4)-connected nets in coordination polymers,[12] the most symmetrical and important examples are boracite, Pt_3O_4,[13] cubic-C_3N_4,[14] and the twisted boracite.[1c] Recently, Moorthy reported a (3,4)-connected net related PtS network with a $(4\ 12^2)_2(4^212^4)$ Schläfli symbol.[15] Therefore, the structure of **4** provides another valuable prototype of (3,4)-connected nets which would be important for the design of MOFs.

The long Schläfli symbol is $6{\cdot}6{\cdot}6{\cdot}6{\cdot}12_2{\cdot}12_2$ for the Eu1 node and $6{\cdot}6{\cdot}10_2$ for the Eu2 node, giving the net symbol $(6{\cdot}6{\cdot}10_2)_2(6{\cdot}6{\cdot}6{\cdot}6{\cdot}12_2{\cdot}12_2)$ which can be represented by the short symbol $(6^210)_2$ (6^410^2). From the topological symbol, it can be seen that the 12-gons represent the largest circuit of the three essential rings (6-gons, 10-gons, 12-gons) that define the topology (Figure 2b and Figure S2). There are two different node−node distances in the network of **4** (Eu1···Eu2 = 4.400 Å, Eu2···Eu2 = 3.925 Å) corresponding to two different types of links.

Photoluminescence Properties. Taking into account the excellent luminescent properties of Eu^{III}, Dy^{III}, and Sm^{III} ions, the luminescences of **2, 4**, and **5** were investigated at room temperature. Excitation of the as-synthesized solid of **4** at 296 nm reveals the characteristic transition of the Eu^{III} ion (Figure 5a). They are attributed to $^5D_0 \rightarrow {}^7F_J$ ($J = 1, 2, 3, 4$) transition, i.e., 592 nm ($^5D_0 \rightarrow {}^7F_1$), 612 nm ($^5D_0 \rightarrow {}^7F_2$), 652 nm ($^5D_0 \rightarrow {}^7F_3$), and 702 nm ($^5D_0 \rightarrow {}^7F_4$). The most intense transition is $^5D_0 \rightarrow {}^7F_2$, which implies a red emission light of **4**. The symmetric forbidden emission $^5D_0 \rightarrow {}^7F_0$ at 580 nm is invisible in **4**. It is well-known that the $^5D_0 \rightarrow {}^7F_0$ transition is strictly forbidden in a field of symmetry. Thus, the above result reveals that Eu^{III} in **4** occupies sites with high symmetry.[16] Complex **2** is yellow-luminescent in the solid state with typical Dy^{III} emission at 480, 572, and 622 nm, corresponding to the characteristic emission $^4F_{9/2} \rightarrow {}^6H_J$ transition of Dy^{III} ion ($J = 15/2$, 13/2, and 11/2; Figure 5b). Excitation of complex **5** at 302 nm leads to the strong pink emission of Sm^{III} due to the $^4G_{5/2} \rightarrow {}^6H_J$ ($J = 5/2$, 7/2, 9/2, and 11/2) transition; the most intense peak is the transition $^4G_{5/2} \rightarrow {}^6H_{7/2}$ at 596 nm (Figure 5c). For all the complexes, the decay is best described by a biexponential process which is consistant with the two extremely different Ln^{III} sites in the structures.[17] The corresponding lifetimes are $\tau_1 = 318$ μs and $\tau_2 = 715$ μs, $\tau_1 = 0.634$ μs and $\tau_2 = 3.14$ μs, and $\tau_1 = 0.512$ μs and $\tau_2 = 2.42$ μs for complex **4**, **2**, and **5**, respectively (Table 3), which are comparable to other corresponding Ln^{III} complexes.[18] With respect to 2,5-H_2pydc, the emission broadband mainly ranges from 350 to 450 nm with one peak at 392 nm.[19] The absence of the ligand-based

Table 3. Photoluminescent Lifetime Data for Compound **2**, **4**, and **5**

	lifetime (μs)	
compound	τ_1	τ_2
4	308 (95.07%)	715 (4.93%)
2	0.634 (23.64%)	3.14 (76.36%)
5	0.512 (15.98%)	2.42 (84.02%)

(12) Batten, R. *CrystEngComm* **2001**, 3, 67−72, and the Web site therein.
(13) Chen, B.; Eddaoudi, M.; Hyde, S. T.; O'Keeffe, M.; Yaghi, O. M. *Science* **2001**, *291*, 1021.
(14) (a) Dybstev, D. N.; Chun, H.; Kim, K. *Chem. Commun*. **2004**, 1594. (b) Bu, X.; Zhang, N.; Li, Y.; Feng, P. *J. Am. Chem. Soc*. **2003**, *125*, 6024.
(15) Natarajan, R.; Savitha, G.; Dominiak, P.; Wozniak, K.; Moorthy, J. N. *Angew. Chem., Int. Ed.* **2005**, *44*, 2115.
(16) (a) Xu, Q. H.; Li, L. S.; Liu, X. S.; Xu, R. R. *Chem. Mater*. **2002**, *14*, 549. (b) Zhao, B.; Chen, X. Y.; Cheng, P.; Liao, D. Z.; Yan, S. P.; Jiang, Z. H. *J. Am. Chem. Soc*. **2004**, *126*, 15394.
(17) Comby, S.; Scopelliti, R.; Lmbert, D.; Charbonnière, L.; Ziessel, R.; Bunzli, J. G. *Inorg. Chem*. **2006**, *45*, 3158.
(18) Quici, S.; Cavazzini, M.; Marzanni, G.; Accorsi, G.; Armaroli, N.; Ventura, B.; Barigellett, F. *Inorg. Chem*. **2005**, *44*, 529.
(19) Song, Y. S.; Yan, B.; Chen, Z. X. *J. Mol Struct*. **2005**, *750* 101.

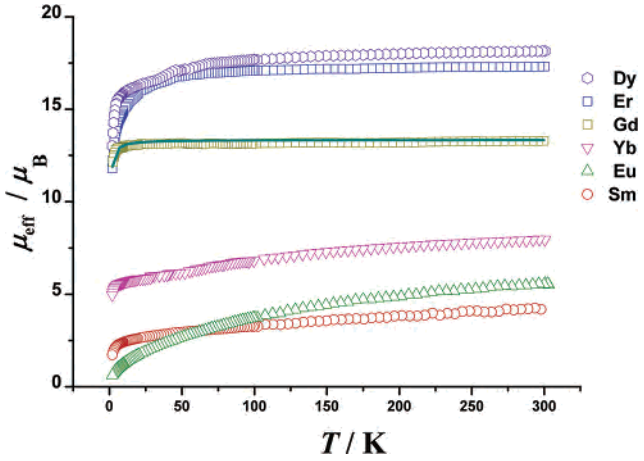

Figure 6. Temperature dependent μ_{eff} versus T plots for **1**−**6**.

emission in the fluorescence spectra of **2**, **4**, and **5** suggests that the energy transfer from the ligand to the lanthanide center is effective. Furthermore, the excitation spectra of **2**, **4**, and **5** show the effective energy absorption mainly takes place in the region 225−350 nm, which matches the absorption spectrum of the ligand; therefore, the ligand-lanthanide ions energy transfer is confirmed (Figure 5d).

Magnetic Properties. The temperature dependencies of effective magnetic moments (μ_{eff}) of complexes **1**−**6** in the temperature range 2−300 K were studied, and the results show that their magnetic properties are very different, though they have the same structures. Figure 6 shows the temperature dependencies of the magnetic susceptibilities in the form of μ_{eff} vs T for complexes **1**−**6**. For complex **1**, in the whole temperature range, the μ_{eff} value is almost constant from 13.29 μ_B to 13.02 μ_B at 13 K and then to 11.82 μ_B at 2 K. The dramatic decrease of μ_{eff} at low temperature is mainly attributed to the weak antiferromagnetic coupling between the Gd^{3+} ions and may also partially arise from the very small splitting of the $^8S_{7/2}$ multiplet at zero field.[20] The Gd1−Gd2 separation of 4.446 Å is quite longer than the Gd2−Gd2 distance 3.908 Å, and, according to the empirical Bloch law $J = d^{-10}$,[21] the coupling between Gd1−Gd2 is about 1 order of magnitude less than the coupling between Gd2−Gd2 and can be neglected for simplification. Therefore, the simple uniform chain model with Hamiltonian $H = -\sum_{i<j} J_{ij} S_i S_j$ and $S = 3.5$ can be used here. The expression of magnetic susceptibility of complex **1** is $\chi_M = 2N\beta^2 g^2/KT$ [$1 + u/1 - u$] where $u = (\exp^{(C)} + \exp^{(-C)})/(\exp^{(C)} - \exp^{(-C)}) - 1/C$, $C = J*3.5*(3.5 + 1)/(0.695*T)$ and N, g, and β have their usual meanings.[22] J is the coupling constant between the Gd2 ions. The best fit by a standard squares-fitting program gives $g = 1.941(2)$, $J = -0.030(3)$ cm^{-1}, and $R = 8.97 \times 10^{-5}$, where $R = \Sigma(\chi_{obs} - \chi_{calc})^2/\Sigma\chi^2_{obs}$. Similar varieties of the temperature dependence of μ_{eff} can also be found in complexes **2** and **3**. However, for complexes **4**−**6**, there are continuous decreases in μ_{eff} as the temperature drops, which mainly indicate the feature of single Ln^{3+} ion.

Conclusions

In summary, a series of novel 3D lanthanide hybrids containing distinct Ln_{12} wheels and clustered nanosized lanthanide oxide ring tunnels have been successfully constructed. The μ_5-pydc coordination in the structures plays a key role in forming and stabilizing the lanthanide oxide tunnels. To the best of our knowledge, compounds **1**−**7** represent the first example of a 3D lanthanide hybrid with lanthanide oxide tunnels and a (3,4)-connected $(6^210)_2$ $(6^4\text{-}10^2)$ net. It is also worth noting that the originality of the structure illustrates the versatility of lanthanide-oxide networks and confirms the plasticity of lanthanide inorganic condensation under hydrothermal conditions. The successful syntheses of compounds **1**−**7** not only provide novel examples of 3-D lanthanide hybrids with (3, 4)-connected nets but also may open up possibilities for the design of new hybrid materials with particular functions.

Acknowledgment. This work was supported by grants from the National Natural Science Foundation of China and the Natural Science Foundation of Fujian Province.

Supporting Information Available: Bond lengths and angles of complexes (Tables S1−S5) and CCDC-613180 (**1**), 613181 (**2**), 602307 (**3**), 602305 (**4**), 602306 (**5**), and 613182 (**7**) with crystallographic data. This material is available free of charge via the Internet at http://pubs.acs.org.

IC0615271

(20) (a) Panagiotopoulos, A.; Zafiropoulos, T. F.; Perlepes, S. P.; Bakalbassis, E.; Massonramade, I.; Kahn, O.; Terzis, A.; Raptopoulou, C. P. *Inorg. Chem.* **1995**, *34*, 4918. (b) Xu, G.; Wang, Z. M.; He, Z.; Lu, Z.; Liao, C. S.; Yan, C. H. *Inorg. Chem.* **2002**, *41*, 6802.

(21) Angelov, S.; Drillon, M.; Zhecheva, E.; Stoyanova, R.; Belaiche, M.; Derory, A.; Herr, A. *Inorg. Chem.* **1992**, *31*, 1514.

(22) Kahn, O. *Molecular Magnetism*; Wiley-VCH: New York, 1993.